IEEE Photonics Journal
An IEEE Photonics Society Publication

Method for Polarization-Resolved Measurement of Electroabsorption

Volume 10, Number 1, February 2018

Dzmitry Pustakhod
Kevin Williams
Xaveer Leijtens

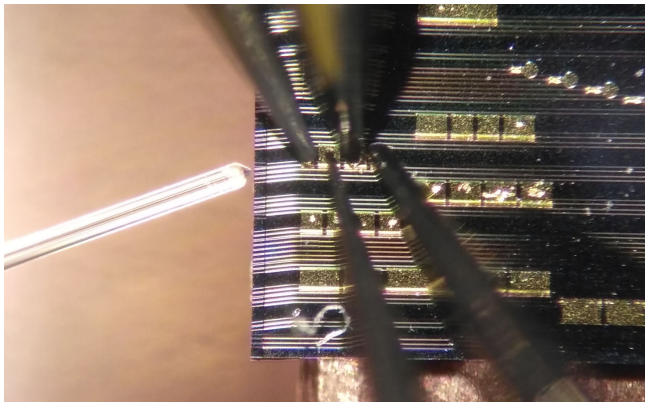

DOI: 10.1109/JPHOT.2018.2795250
1943-0655 © 2018 CCBY

IEEE photonics SOCIETY

IEEE

Method for Polarization-Resolved Measurement of Electroabsorption

Dzmitry Pustakhod, Kevin Williams, and Xaveer Leijtens

Institute of Photonic Integration, Photonic Integration Group, Department of Electrical Engineering, Eindhoven University of Technology, Eindhoven 5600 MB, The Netherlands

DOI:10.1109/JPHOT.2018.2795250

Manuscript received November 24, 2017; revised January 12, 2018; accepted January 15, 2018. Date of publication January 23, 2018; date of current version February 27, 2018. This work was carried out in the ProCon Project 11369, supported by the Dutch Technology Foundation STW, which is part of the Netherlands Organization for Scientific Research (NWO), and which is funded by the Dutch Ministry of Economic Affairs. Corresponding author: Dzmitry Pustakhod (e-mail: d.pustakhod@tue.nl).

Abstract: Photonic integrated circuits often use semiconductor components such as amplifiers, detectors, and electroabsorption modulators. For a proper circuit design, it is important to know the absorption spectrum of these semiconductor optical components and how it depends on an applied electric field. We propose a fast and accurate method that uses a compact segmented contact structure to measure the absorption characteristics. The method is based on measuring the transmission of amplified spontaneous emission (ASE) from a single forward-biased section through a varying number of reversely biased absorbing sections. Provided the ASE source emits light in both polarizations, the method measures the absorption spectra for both polarization modes simultaneously, without the need for a polarization filter in the measurement setup.

Index Terms: Absorption measurement, semiconductor optical amplifiers, photonic integrated circuits, segmented device, active-passive integration, polarization.

1. Introduction

The electro-absorption spectrum is an important parameter of various semiconductor devices, such as electro-absorption modulators (EAMs), photodetectors, and integrated semiconductor optical amplifiers (SOAs). Knowledge about the absorption is needed for designing and simulation of complex circuits, for example mode-locked lasers or integrated wavelength meters. Currently there is an increasing interest in on-chip polarization handling, e.g., in dual polarization transmission systems [1], [2]. The measured absorption can also be used for testing purposes to extract semiconductor material parameters [3]. This requires methods for polarization-resolved measurement of absorption spectra.

A number of different methods have been proposed to measure absorption spectra. The transmission method is based on comparison of the transmitted light spectrum with a known incident spectrum. Polarization dependency is usually measured by a matrix technique, also known as Mueller–Stokes technique [4]. This method requires an external swept-wavelength light source together with a polarization state generator. However, the calculated absorption includes the coupling efficiency, which has to be measured precisely to decouple it from the absorption in the device itself.

Several methods employing an integrated source were suggested to overcome this limitation. They are based on analysis of the amplified spontaneous emission (ASE) spectra from segmented SOAs, where the external source is replaced by one of the sections of the device [5], [6]. The

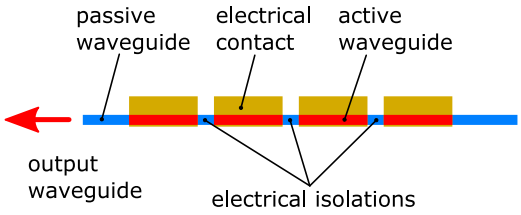

Fig. 1. Schematic diagram of a multisection device. Light is collected through the output waveguide. The waveguide on the other side of the device should be designed in a way to ensure no returning light back into the device (e.g., terminated with an absorber).

absorption can be calculated from the incident and transmitted light intensities for one absorber length [6], or from the fit of the transmitted light intensity for multiple absorber lengths [5]. A modification of the method was suggested by Xin *et al.* [7] in order to exclude the contribution of unguided spontaneous emission from the structure. This unguided radiation can also be avoided by using a single-mode fiber to collect the emitted light. Such a fiber serves as a spatial filter and collects only the light mode propagating in the waveguide.

In order to obtain the absorption spectrum for a particular polarization, all mentioned methods use a polarizer in the detection system to measure only the corresponding polarization mode. In a fiber-based collection system, the tolerances on standard connectors do not allow to maintain accurate angular alignment, limiting the crosstalk between modes to around —20 dB. Thus, in case of relatively low spontaneous emission intensity into one of the modes, there is a significant fraction of the other mode left after filtering, which brings a systematic error to the measured absorption. We propose a modification of the segmented method to measure both TE and TM modal absorption at the same time without using polarization filtering in the collection system.

The proposed method is based on the measurement of transmitted broadband light through a series of absorbers of different lengths with an optical spectrum analyzer (OSA). The emission spectrum of the light source should be known, and it should contain emission in both polarizations. However, when using a multisection device as is done in this paper, the emission spectrum does not need to be known in advance, as it is measured from the same test structure. The method makes use of the difference in absorption in the two polarization modes.

This paper is organized as follows. In the next section, we introduce in detail the structure to be used in the measurements, and the relations describing the optical power spectra emitted by multi-section SOAs. In Section 3, we describe the proposed method for the absorption calculation. Besides this, we briefly describe the reference method from [6] which we use to verify the results. In Section 4 we describe the structure design and fabrication followed by the description of the measurement setup. In Section 5 we present the measurement results from both the proposed and the reference method and discuss them.

2. Test Structure Description

For the measurements, a broadband light source emitting into both polarizations is needed. When measuring semiconductor devices, we can exploit the property that they experience both absorption and emission depending on the applied voltage or current direction. Therefore we can use a segmented structure. A similar test structure with SOAs serving as individual sections was used previously for SOA gain measurements [6]–[9]. One of the advantages of such structure is that only one optical alignment is needed, which helps to speed up the measurement and reduces errors related with the coupling variation. In this paper we will demonstrate the proposed method with a multi-section structure for measuring semiconductor absorption.

A schematic of a segmented structure is shown in Fig. 1. The structure consists of a number of SOAs connected by passive waveguides. In this paper we use the same term “SOA” for both the ASE sources (forward bias) and for the absorbers (reverse bias). Each SOA contains an optically active material and a metal pad for applying electrical signal to it. The SOA sections are

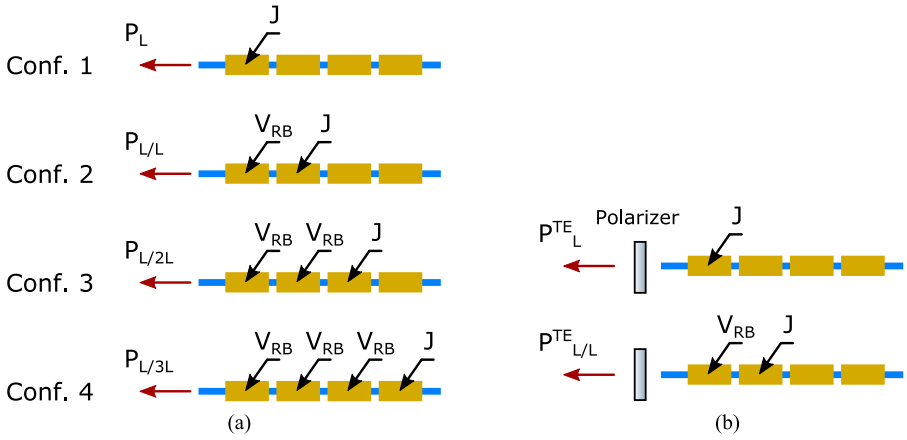

Fig. 2. (a) Measurement configurations for the proposed polarization resolved absorption measurement method. (b) Measurement configurations for the reference absorption measurement method. Only the measurement with the polarizer aligned to transmit the TE mode is shown. All sections have the same length L.

electrically isolated from each other, in order to be able to pump or reverse bias them independently. The waveguide outside of the SOA is passive and has negligible optical loss compared to the active waveguide. During the measurement, light is always collected from the same output waveguide through the front facet. The structure should have no internal reflections, e.g., between the active and passive waveguides. Any reflections from facets back into the structure should also be avoided to guarantee single pass of light through it.

With such structure, both the ASE spectrum and the spectrum after absorption can be obtained by applying different combinations of pump current J and reverse bias V_{RB} to the SOA sections. Examples of such configurations are shown in Fig. 2. The effective length of absorber can be changed by changing the number of reverse biased sections.

2.1 Amplified Spontaneous Emission

In the general case, a directly biased SOA section with a current density J emits light into the TE and TM polarization modes. For each of the modes, the spectral distribution is determined by the corresponding spontaneous emission spectrum $p_{\mathrm{sp}}(\lambda, J)$ and the gain spectrum $g(\lambda, J)$ (both per unit length). For example, the ASE spectrum into TE mode $P^{TE}_{\mathrm{ASE}}(\lambda, J)$ can be calculated as [10]:

$$P^{TE}_{\mathrm{ASE}} = P^{TE}_{L_e} = \frac{p^{TE}_{\mathrm{sp}}}{g^{TE}}(e^{g^{TE}L_e} - 1), \tag{1}$$

where L_e is the length of the emitter.[1] The spontaneous emission intensity and gain for a particular structure depend on the applied current density through the SOA. The total optical power spectrum can be described as a sum of powers in these modes:

$$P_{L_e} = P^{TE}_{L_e} + P^{TM}_{L_e}, \tag{2}$$

where $P^{TE}_{L_e}$ and $P^{TM}_{L_e}$ are the total power emitted into TE and TM mode respectively. We will refer to the ratio of powers in two modes as

$$R_{L_e}(\lambda, J) = P^{TE}_{L_e}/P^{TM}_{L_e}. \tag{3}$$

The power ratio R_{L_e} is useful to compare emission into the two polarization modes, and we will use it later when presenting the results. In equations, however, it is more practical to use a related

[1]In the subsequent notations we will often omit the explicit wavelength and current density dependence of spectral quantities, e.g., we will use g^{TE} for $g^{TE}(\lambda, J)$.

quantity r_{L_e}, which describes the fraction of the power in the TE mode and is defined as

$$r_{L_e} = \frac{P_{L_e}^{TE}}{P_{L_e}} = \frac{R_{L_e}}{(R_{L_e}+1)} \tag{4}$$

Note that the power ratio R_{L_e} can be directly calculated from the TE power fraction r_{L_e}: $R_{L_e} = r_{L_e}/(1 - r_{L_e})$ For a given emitter length L_e, ratios $R_{L_e}(\lambda, J)$ and $r_{L_e}(\lambda, J)$ vary with wavelength, and are dependent on the pump current density J.

2.2 Transmission Through an Absorber

An SOA section of length L_a with an applied reverse bias voltage V_{RB} will absorb part of the light that is entering the section. The amount of the transmitted power spectrum P_t is characterized by the mode absorption spectra $\alpha^{TE}(\lambda, V_{RB})$ and $\alpha^{TM}(\lambda, V_{RB})$ according to Beer's law [11]. For example, for the TE mode:

$$P_t^{TE} = P_i^{TE} e^{-\alpha^{TE} L_a} = P_i^{TE} \eta_{L_a}^{TE}, \tag{5}$$

where P_i^{TE} is the incident optical power spectrum in TE mode, and $\eta_{L_a}^{TE}(\lambda, V_{RB}) = e^{-\alpha^{TE}(\lambda, V_{RB}) L_a}$ is the modal transmittance of the SOA section with a given length. Similar to ASE case, the total power spectrum $P_t(\lambda, J, V_{RB})$ is calculated as a sum of powers in two modes:

$$P_t = P_t^{TE} + P_t^{TM} = P_i^{TE} \eta_{L_a}^{TE} + P_i^{TM} \eta_{L_a}^{TM}, \tag{6}$$

3. Absorption Calculation Methods

3.1 Measurement Configurations of a Segmented Device

When using a multi-section device, we apply a pump current and a reverse bias to the SOA sections independently. The corresponding configurations for the proposed and reference methods are shown in Fig. 2(a) and (b). All sections of the test structure have the same length L. The spectrum of the first configuration in Fig. 2(a), P_L, is described by (2) with $L_e = L$.

In the second configuration, we pump Section 2 and apply a reverse bias to absorbing Section 1: $L_e = L_a = L$ with L_a the length of the absorber. The absorption calculation is based on the assumption that the ASE spectrum emitted by Section 1 is identical to the ASE spectrum emitted by Section 2 in the direction of Section 1, if both sections have the same length. This means that the incident power to the absorbing section P_i is the same as the emitted by Section 1 in previous configuration: $P_i^{TE} = P_L^{TE}$, $P_i^{TM} = P_L^{TM}$. From (6):

$$P_t = P_{L_e/L_a} = P_{L/L} = P_L^{TE} \eta_L^{TE} + P_L^{TM} \eta_L^{TM}. \tag{7}$$

In the notation used, P_{L_e/L_a}, first part of subscript, L_e, refers to the length of the pumped emitting SOA, and the second part, L_a, refers to the length of the absorbing section.

3.2 Polarization-Resolved Method

We studied two methods to derive the absorption spectra from the measurement data. Both of them use data from a similar measurement procedure, but data analysis is done in a different way. The first one is based on solving a system of nonlinear equations at a single reverse bias voltage (direct extraction), the other one uses nonlinear regression on the data measured at multiple reverse bias voltages. Both methods are described below.

3.2.1 Method I—Direct Extraction: During the measurement, four optical power spectra are measured. They are generated by the combinations of pump current and reverse bias of SOAs as is shown in Fig. 2(a). The pump current and reverse bias voltage values are the same for all configurations. For each configuration, the total power is a sum of powers in TE and TM modes.

Using (2) and (7), the collected power can be described by the following set of equations:

$$\begin{aligned} P_L &= P_L^{TE} + P_L^{TM}, \\ P_{L/L} &= P_L^{TE}\eta_L^{TE} + P_L^{TM}\eta_L^{TM}, \\ P_{L/2L} &= P_L^{TE}\eta_{2L}^{TE} + P_L^{TM}\eta_{2L}^{TM}, \\ P_{L/3L} &= P_L^{TE}\eta_{3L}^{TE} + P_L^{TM}\eta_{3L}^{TM}. \end{aligned} \tag{8}$$

For convenience, we will use ratio $\delta_{L_a}(\lambda, J, V_{RB}) = P_{L/L_a}/P_L$, which characterizes the fraction of total power transmitted through the absorber. We rewrite (8) in the following way:

$$\begin{aligned} \delta_L &= r\eta_L^{TE} + (1-r)\eta_L^{TM}, \\ \delta_{2L} &= r(\eta_L^{TE})^2 + (1-r)(\eta_L^{TM})^2, \\ \delta_{3L} &= r(\eta_L^{TE})^3 + (1-r)(\eta_L^{TM})^3, \end{aligned} \tag{9}$$

where the fraction of power in TE mode r is defined by (4).

Therefore, after measuring 4 configurations depicted in Fig. 2(a) for a given pump current density J and reverse bias voltage V_{RB}, at each wavelength we obtain a system of three nonlinear equations with three unknowns r, η_{TE}, and η_{TM}. The numerical solution of this system at every wavelength gives the polarization power ratio in the ASE emitted by a single section R and the absorption spectra of the TE and TM modes α_{TE} and α_{TM}. To summarize, this calculation method requires 4 data points, and yields 3 parameters as a solution.

It is not known to which of the two modes, TE or TM, the two absorption values obtained from the solution of (9) correspond. They can be identified with additional knowledge about the layer stack and the structure, or from a measurement with an external polarization filter, such as described in Section 5.2.

3.2.2 Method II—Nonlinear Regression: This method is a more advanced technique, which makes use of measurement data from multiple reverse bias voltage values V_{RB}. As was mentioned in Section 2.1, one of the unknowns in the system (9), the ratio r, at a given wavelength, is determined only by the current density J. It is independent of V_{RB} applied to other sections of the test structure. This property is used to reduce the number of unknowns compared to the number of measured data points. By applying a nonlinear regression approach (fitting), it is possible to reduce the error and uncertainty of the result.

First, we measure one spectrum of configuration 1. Additionally, we measure three spectra of configurations 2 to 4 for each of K reverse bias voltages $V_{RB,k}$. The number of data points totals to $3K + 1$, giving a set of $3K$ values for transmitted power fractions δ_{L_a}.

The TE and TM modal absorption are different for each reverse bias value applied to the absorber sections while the ratio r for the light from the emitter stays the same. The number of unknowns is therefore $2K + 1$, which includes one value for ratio r, and K values for each of the transmittances $\eta_{L,k}^{TE}$ and $\eta_{L,k}^{TM}$. Therefore, the number of equations exceeds the number of unknown parameters for $K \geq 2$, and nonlinear regression is used to determine optimum parameter values.

The model for nonlinear regression is described by (9). The transmitted power fraction δ_{L_a} is the dependent variable, while ratio r and the transmittances $\eta_{L,k}^{TE}$ and $\eta_{L,k}^{TM}$ are the unknown model parameters.

3.3 Reference Method With Explicit Polarization Filtering

In order to validate our method, we use a reference method that employs multiple absorber lengths and a polarization filter in the measurement system. This method was described and used in [5] and [6]. We compare the absorption spectra measured with our method with those obtained by the reference method. The pump and bias configurations for the reference method are shown in Fig. 2(b). The measurement setup should include a polarization filter, which is aligned with the TE or TM mode in the waveguide. It is needed to filter out the other polarization mode.

To obtain the modal absorption, we compare the ASE spectrum in the selected polarization mode from the first SOA section P_L^{TE}, and the power spectrum $P_{L/L}^{TE}$ from the second SOA section of the same length, passing through a reversely biased absorber, we can calculate the TE absorption in the following way:

$$\alpha^{TE} = -\frac{1}{L_a} \ln\left(\frac{P_{L/L}^{TE}}{P_L^{TE}}\right). \tag{10}$$

The above equation is given for the TE mode being transmitted through the filter, but the same is applied for the TM mode.

To obtain absorption spectra for K values of the reverse bias, $K + 1$ measurements are required for each polarization.

4. Fabrication and Measurement

4.1 Structure Design and Fabrication

In our experiment we used the InP-based test structures fabricated by Smart Photonics in a multi-project wafer (MPW) run through the JePPIX.eu open access service [12]. This platform uses a butt-joint active-passive integration, which allows the lengths of active sections to be varied independently of the chip size. The layer stack for the passive waveguides uses bulk InGaAsP (Q1.25) as core material with InP as a cladding. The active layer stack contains 4 InGaAsP quantum wells optimized for emission at 1550 nm [13].

The multi-section test structure used in the experiment consists of a single waveguide with several SOA sections separated by passive electrical isolation sections. Its design is the same as used for the SOA gain measurements that were previously reported in [9]. The structure is composed of three building blocks provided in the Process Design Kit by the foundry: shallow passive waveguides, SOAs (gain sections), and passive electrical isolation sections [13]. All waveguides are shallow etched ridge waveguides of 2 μm in width. The typical loss of the passive waveguide is 2 dB/cm. The length of active sections is 100 μm. The separating isolation sections have part of p-doped InP top cladding removed [13]. The length of isolation sections is 30 μm, and they provide 0.7 MΩ resistance. We used *passive* isolation sections, because it is important to have low loss in them compared to the components under test. More details on the technology and the building block composition and performance are available in a paper by L. Augustin *et al.* [13].

4.2 Measurement Setup

In the measurement setup (Fig. 3), the chip is epoxy-bonded to a copper chuck. In order to keep the chip temperature constant at different current densities, an active cooling by a thermo-electrical cooler (TEC) and a thermocontroller with a Thorlabs Pro8000 Mainframe is used. Electrical signals from the source meters are provided through the individual electrical probes contacting the metal pads of the SOA sections.

A top-view microphotograph of the chip installed on the measurement setup is shown in Fig. 4. The measured structure consists of four SOA sections each having the same length of 100 μm. The electric probe needles are landed on the SOA contact pads and connected to the source meter. The output waveguides are made at a 7° angle to suppress back reflection into the structure. The lensed fiber to the left of the chip is aligned to the waveguide facet.

Light emitted by the SOAs is collected through the chip facet with a single-mode lensed optical fiber. The fiber is mounted on the 3-axis piezo positioner, which allows accurate fiber alignment to the waveguide. To accommodate the temperature expansion of the mount and to keep the coupling efficiency from the integrated waveguide to the lensed fiber constant, the fiber tip is realigned after each current setting. The lensed fiber serves as a spatial filter and prevents collection of unguided light into the measurement system. This was shown in [9], where we used the same setup and verified good agreement of the measured emission intensity with the model.

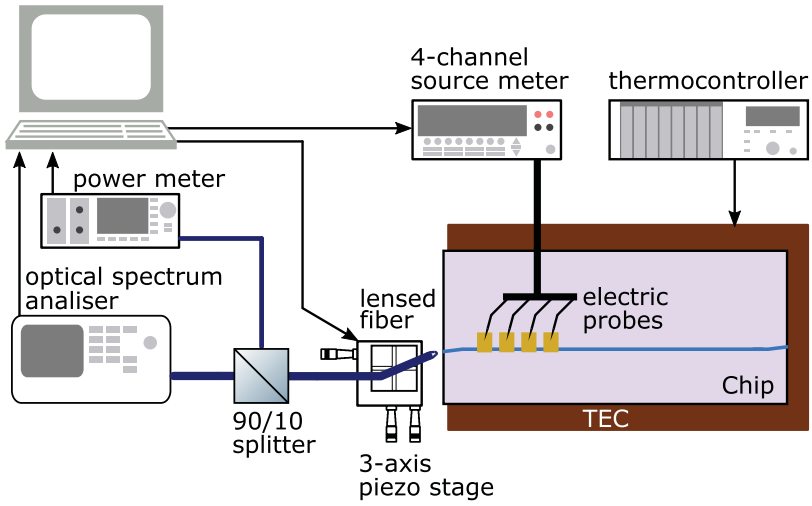

Fig. 3. Schematic of the setup for polarization-resolved absorption measurement. TEC—thermoelectric cooler. The same setup with an additional polarization filter in combination with polarization-maintaining fiber was used for the reference method.

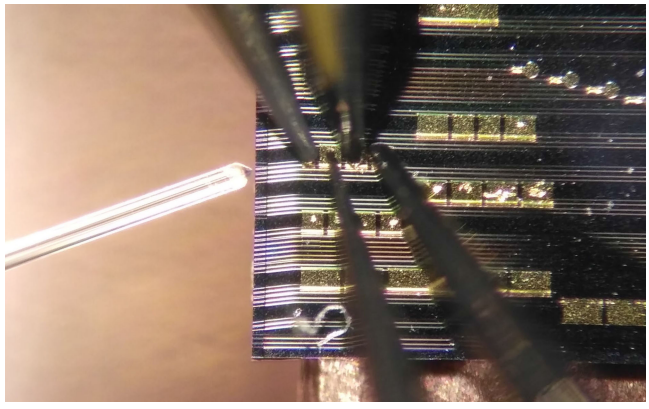

Fig. 4. Micrograph of the chip with test structures manufactured in an MPW run by Smart Photonics. The chip is installed on a copper chuck and four electrical probe needles are contacting the pads of the structure. The lensed fiber is aligned to the angled output waveguide.

The collected light is then directed to an optical spectrum analyzer ANDO AQ-6315A, which measures the resulting ASE spectrum with a resolution setting of 0.5 nm. The OSA noise floor at the used sensitivity was measured to be $P_{\text{noise}} = -90\,\text{dBm}$, and its measurement uncertainty is $\epsilon = 0.3\,\text{dB}$ from the equipment specification.

The power detected at each wavelength is determined by the resolution setting, while the OSA noise floor is independent of it. Therefore, the spectral density values presented in this paper are in dBm/res units, while the noise floor is measured in dBm. The resolution setting can be adjusted to increase the signal to noise ratio at the expense of small features in the spectrum.

5. Measurement Results

5.1 Polarization Resolved Measurement

5.1.1 Method I—Direct Extraction: First, we have used the direct absorption extraction method by solving the system of nonlinear equations (9) at a single reverse bias voltage, as described in Section 3.2.1.

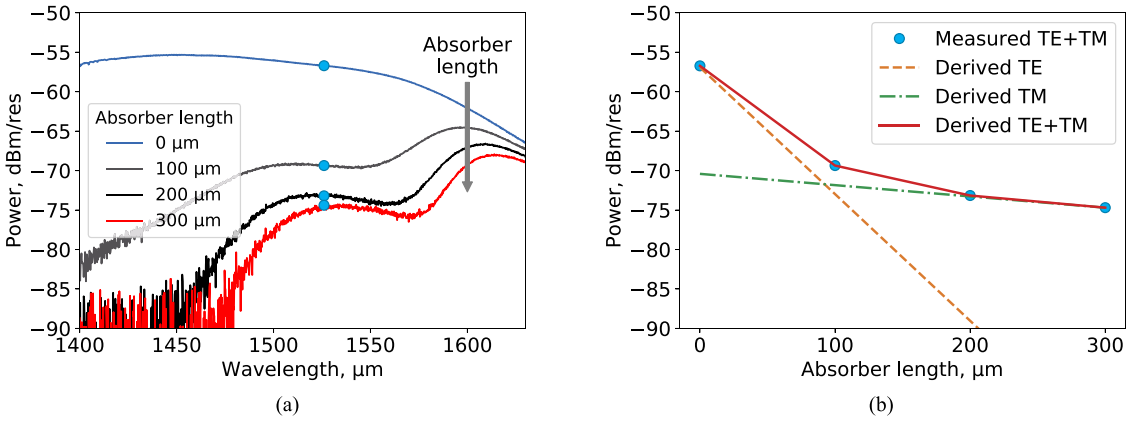

Fig. 5. (a) Measured ASE spectra, configurations 1 to 4, for pump current density $J = 10\,\mathrm{kA/cm^2}$, emitter length $L_e = 100\,\mu$m. Absorber is biased at voltage $V_{RB} = -5\,\mathrm{V}$ and its total length L_a varies from 0 to 300 μm. (b) Measured ASE at 1526 nm (blue), and derived polarization-resolved ASE (TE—orange, TM—green) power spectral density values. The OSA resolution used is 0.5 nm.

After setting a pump current density and reverse bias on the corresponding sections according to the configurations shown in Fig. 2, we record the resulting spectra from the OSA. An example of the measured spectra from the test structure with section lengths of 100 μm is shown in Fig. 5(a). The setting for the pump current density is $J = 10\,\mathrm{kA/cm^2}$. We have selected this maximum nominal value for the used platform to achieve higher signal intensity and improve the signal-to-noise ratio. The reverse bias is set to be $V_{RB} = -5\,\mathrm{V}$. The top curve corresponds to the ASE P_L from the first section. The three lower curves are the ASE spectra P_{L/L_a} for three different total absorber lengths ($L_a = 100, 200, 300\,\mu$m). Therefore, we have four measured values of the power spectral density at each wavelength to be used in absorption calculation.

As an example of the calculation procedure, Fig. 5(b) shows the values at 1526 nm from Fig. 5(a) with blue circles (-56.71, -69.36, -73.2, -74.39 dBm/res). These values were used to calculate the fraction of power transmitted through the absorber δ_{L_a} for the (9). The numerical solution of these equations brings the values for the TE/TM ratio R and for the modal absorptions α_{TE} and α_{TM} at the selected wavelength.

The transmitted power for the TE and TM modes, calculated from the solution, is shown in Fig. 5(b) in orange and green respectively. The TE mode is dominant in the ASE spectrum measured directly without absorbing sections. This is expected, as in the platform used, the layer stack is optimized for higher gain for the TE mode. Due to the higher TE modal absorption, the power in the TE mode rapidly decreases with an increase of the absorption length. In contrast, the TM-mode power drops much slower and prevails in the spectrum measured through a long absorber. The sum of two represents the total measured power shown in blue. This plot demonstrates that two important properties of the measured devices are enabling the convergence of solution of (9). They are a significant TE/TM power ratio R in the ASE spectrum and a difference between modal absorption coefficients.

We have performed spectral measurements for six values of reverse bias V_{RB} in the range from 0 to -5 V. For each reverse bias and at each wavelength, the nonlinear system (9) was solved to obtain solutions plotted in Fig. 6.

Fig. 6(a) shows the power ratio of TE and TM modes $R_L(\lambda, J)$ in the ASE spectrum of a single SOA section. The plot shows that the extracted ratio R does not depend on the applied to the absorber reverse bias voltage, which is expected and confirms the validity of the solution. This also justifies the applicability of the second proposed derivation method via nonlinear regression, which relies on the ratio R being independent of the reverse bias as discussed previously in Section 3.2.2.

Fig. 6(b) shows modal absorption spectra for TE and TM modes at different reverse bias. The TE absorption is higher than the TM absorption in the whole range where the algorithm converges

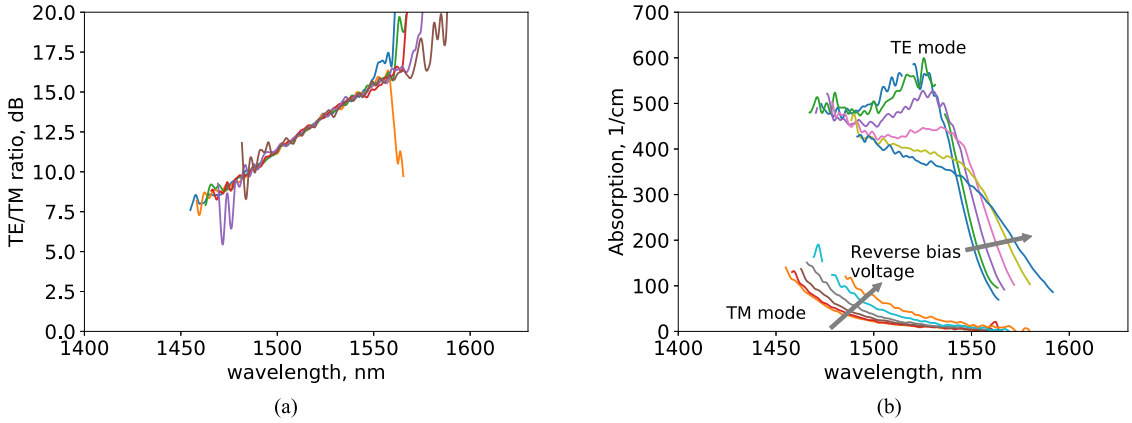

Fig. 6. Experimentally derived TE/TM ratio in the ASE spectrum of a single SOA section (a) and TE and TM modal absorption (b) for the reverse bias voltages from 0 to −5 V. The direct extraction method through solving a nonlinear system at each voltage was used. The 100 μm-long SOA section was pumped to 10 kA/cm^2. All plots were smoothed with a moving average filter.

to a solution. The TE absorption spectra shift towards higher wavelength as expected due to the quantum confined Stark effect [14].

Due to the high absorption at shorter wavelengths, the transmitted power appears to be lower than the sensitivity of the OSA limits (see Fig. 5(a)). This limits the range of the method at lower wavelengths. Thus, for the results shown in Fig. 6, the measured power values below −85 dBm/res were discarded. By contrast, at longer wavelengths, TE and TM transmittance η_L^{TE} and η_L^{TM} are low, but they have a similar value. Therefore the numeric algorithm for solving nonlinear system (9) fails to converge. Moreover, the calculated transmittance η_L^{TM} has negative values in the range from 1550 to 1600 nm, which is not a physical solution of the system.

5.1.2. Method II—Nonlinear Regression: The second method we used is the nonlinear regression on measurement data for all reverse bias values as described in the Section 3.2.2.

In the experiment, we have measured ASE spectra transmitted through absorber sections at six values of reverse bias voltage in the range from 0 to −5 V. Similar to the direct extraction with method I, the regression is performed sequentially on measured power density values at each wavelength to obtain the spectral distribution of the parameters $r(\lambda)$, $\eta_L^{TE}(\lambda, V_{\mathrm{RB}})$ and $\eta_L^{TE}(\lambda, V_{\mathrm{RB}})$. The LMFIT python package [15] was used to find the optimum parameter values.

While performing the regression, we introduced several constraints on the unknowns in the (9). First, the ratio r is subject to the condition $0 < r < 0.5$, which is equivalent to the condition $R_{L_e} = P_{L_e}^{TE}/P_{L_e}^{TM} > 1$. It means that an SOA emits more power into the TE mode than to the TM mode, which is known to be the case for this specific material and was confirmed by the measurement result shown in Fig. 6(a). Second, for the measured SOA layer structure, we expect TE absorption to be higher than the TM absorption: $\eta_L^{TE} < \eta_L^{TM}$. To ensure this condition, we substitute η_L^{TM} in (9) by $\rho\,\eta_L^{TE}$, and $\rho(\lambda, V_{\mathrm{RB}})$ is required to be greater than unity. As a last modification, we have used a moving average filter on the measured spectra, which is equivalent to increasing OSA filter function width by factor of 5. This leads to a reduction of noise in the data at the expense of spectral resolution. Introduction of these constraints made it possible to find a physical solution in a broader range of wavelengths, especially at higher wavelengths.

The derived result for the TE/TM power ratio R in the emitter ASE is shown in Fig. 7(a). The obtained values have smaller variation than for the calculated values for each reverse bias independently, compared with the results presented in Fig. 6(a). The corresponding absorption spectra for both polarizations are shown in Fig. 7(b).

On the resulting spectra (Fig. 7) we can mark three different regions. At the lower wavelengths (region I), the absorption in both TE and TM modes is high. Due to that, the registered power by OSA in this range is below its sensitivity, especially for longer absorbers. Therefore, the signal is buried

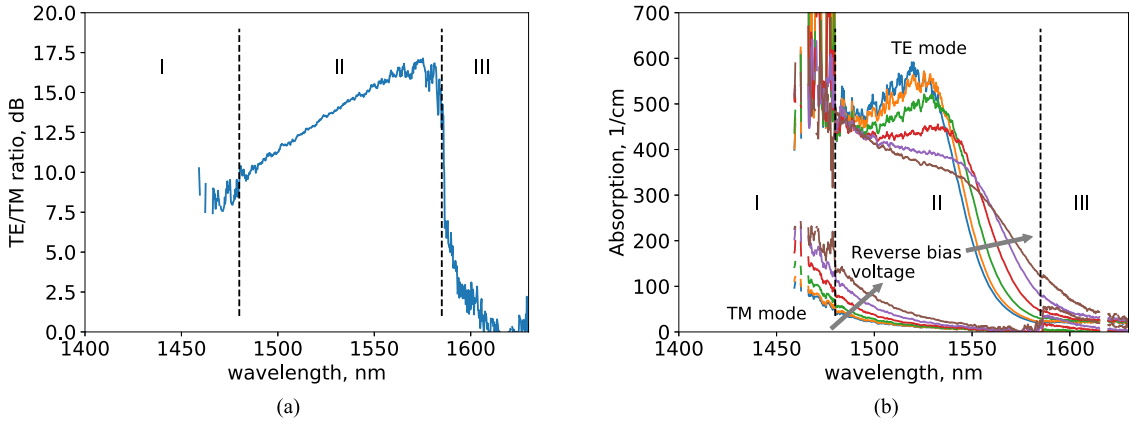

Fig. 7. Optimum fit parameters derived with nonlinear regression method for the reverse bias voltage from 0 to −5 V. (a) TE/TM ratio in the ASE spectrum of a 100 μm-long SOA section pumped to 10 kA/cm^2. (b) TE and TM absorption.

in the measurement system noise. We have discarded the power values below −95 dBm/res, and were not performing regression at those wavelengths. In general, when designing the structure, the section lengths should be selected in the way that the expected transmitted power in the wavelength range of interest is above the sensitivity limit of the OSA.

In the second region covering part of the L–band and the C–band, the nonlinear regression method consistently converges and gives the result with least variation, as the TM mode absorption is significantly smaller than that of TE mode. In region III, which spans beyond 1590 nm, the TE mode absorption drops and becomes similar to the TM mode absorption. Besides that, the amount of light emitted into both modes also becomes comparable. The conditions for the regression algorithm to converge are not fulfilled anymore: although a solution can still be found, it has a higher variation.

5.2 Measurement Validation Using Direct Polarized Absorption Measurement

In order to verify the results obtained with our methods, we have performed the measurement of absorption in both polarizations using the reference method as described in Section 3.3. A polarization-maintaining fiber and a polarization filter were included in the measurements setup (Fig. 3). The axis of the polarization-maintaining fiber was aligned parallel to the optical table and the sample substrate using a free space optical setup, which includes an objective lens, a calibrated polarization filter with a known axis direction, and a photodetector. The extinction ratio of the fiber-based polarization filter was measured to be oscillating in the range from 20 to 25 dB over the whole wavelength range.

The comparison of the absorption spectra obtained with the regression method and the reference method is shown in Fig. 8.

Fig. 8(a) shows absorption spectra for the TE mode at two reverse bias voltages: 0 and −5 V. The results agree with each other with a relative error less than 10 % in the region II. This confirms the accuracy of the values obtained with the regression method.

Fig. 8(b) compares the derived absorption spectra for the TM mode at the same reverse bias voltages. The ripple on the TM absorption measured with the reference method is due to the limited extinction ratio of the fiber-based polarization filter and the strong power ratio (10 to 17 dB from Fig. 7) in the TE and TM ASE. Taking into account the limited polarization filter extinction ratio, this results in the measured power $P_L^{TM}(\lambda)$ from (10) containing a significant fraction of TE-polarized light. The value for TM absorption α^{TM}, derived from (10), is therefore higher than the real one. Our method, in contrast, does not require any polarization filter, which makes the setup simpler and reduces the measurement effort by 50%. Moreover, the result is not affected by the limited extinction ratio of the filter.

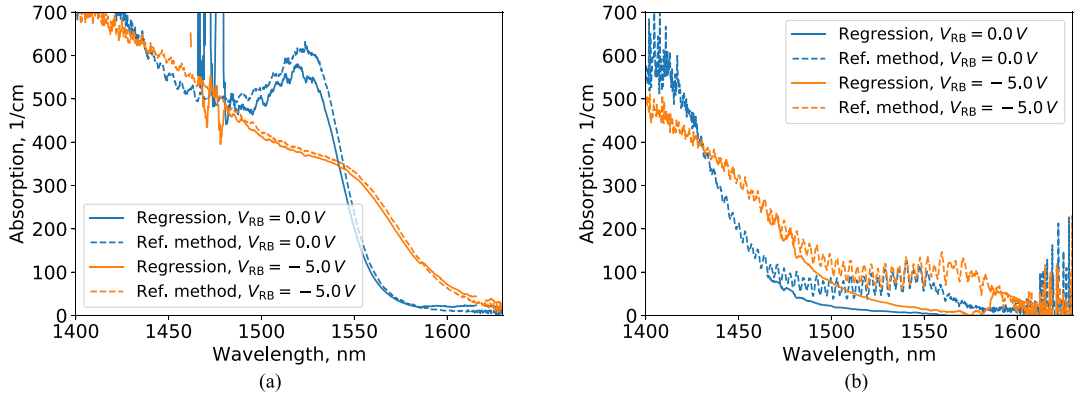

Fig. 8. Comparison of derived absorption spectra with polarization-resolved nonlinear regression method (solid) and reference method with explicit polarization filtering (dashed). (a) TE mode absorption, (b) TM mode absorption. Reverse bias voltage shown are 0 and −5 V.

6. Conclusion

We have presented a method for polarization-resolved absorption measurement. The method is based on the nonlinear regression of the ASE spectra transmitted through absorber sections of various lengths. It can be applied to any device with a significant difference in absorption for orthogonal polarization modes. A practical implementation of the method using a multisection device was presented in the paper. We have shown that the TE and TM modal absorption obtained with this method agree with a reference method which uses off-chip polarization-resolved detection that requires additional polarization control in the measurement setup. Our method is therefore simpler to use and gives comparable or better results, especially for the weaker TM-mode.

References

[1] S. Gaiarin *et al.*, "Experimental demonstration of dual polarization nonlinear frequency division multiplexed optical transmission system," in *Proc. 43rd Eur. Conf. Opt. Commun.*, Sep. 2017, Paper W.3.C.2.
[2] M. Baier *et al.*, "112 Gb/s PDM-PAM4 generation and 80 km transmission using a novel monolithically integrated dual-polarization electro-absorption modulator InP PIC," in *Proc. 43rd Eur. Conf. Opt. Commun.*, Sep. 2017, Paper Th.1.C.3.
[3] C. L. Cesar *et al.*, "Detailed characterization of HgCdTe/CdTe multiple quantum wells," *Appl. Phys. Lett.*, vol. 56, no. 3, pp. 283–285, 1990.
[4] R. M. Craig, "Accurate spectral characterization of polarization-dependent loss," *J. Lightw. Technol.*, vol. 21, no. 2, pp. 432–437, Feb. 2003.
[5] J. Thomson *et al.*, "Determination of single-pass optical gain and internal loss using a multisection device," *Appl. Phys. Lett.*, vol. 75, no. 17, pp. 2527–2529, Oct. 1999.
[6] P. Blood, G. M. Lewis, P. M. Smowton, H. Summers, J. Thomson, and J. Lutti, "Characterization of semiconductor laser gain media by the segmented contact method," *IEEE J. Sel. Topics Quantum Electron.*, vol. 9, no. 5, pp. 1275–1282, Sep. 2003.
[7] Y.-C. Xin *et al.*, "Optical gain and absorption of quantum dots measured using an alternative segmented contact method," *IEEE J. Quantum Electron.*, vol. 42, no. 7, pp. 725–732, Jul. 2006.
[8] S. D. McDougall and C. N. Ironside, "Measurements of reverse and forward bias absorption and gain spectra in semiconductor laser material," *Electron. Lett.*, vol. 31, no. 25, pp. 2179–2181, Dec 1995.
[9] D. Pustakhod, K. Williams, and X. Leijtens, "Fast and robust method for measuring semiconductor optical amplifier gain," *IEEE J. Sel. Topics Quantum Electron.*, vol. 24, no. 1, pp. 1–9, Jan. 2018.
[10] A. Oster, G. Erbert, and H. Wenzel, "Gain spectra measurements by a variable stripe length method with current injection," *Electron. Lett.*, vol. 33, no. 10, pp. 864–866, 1997.
[11] M. Born and E. Wolf, *Principles of Optics*, 6th ed. New York, NY, USA: Pergamon Press, 1993.
[12] X. Leijtens, "JePPIX: the platform for InP-based photonics," *IET Optoelectron.*, vol. 5, no. 5, pp. 202–206, 2011.
[13] L. M. Augustin *et al.*, "In p-based generic foundry platform for photonic integrated circuits," *IEEE J. Sel. Topics Quantum Electron.*, vol. 24, no. 1, pp. 1–10, Jan. 2018.
[14] L. Coldren and S. Corzine, "Diode lasers and photonic integrated circuits," in *Wiley Series in Microwave and Optical Engineering*. New York, NY, USA: Wiley, 1995.
[15] M. Newville *et al.*, "LMFIT: Non-linear least-square minimization and curve-fitting for Python," Sep. 2014. [Online]. Available: https://doi.org/10.5281/zenodo.11813